Chaotic Time-Delay Signature Suppression in a Semiconductor Laser With Frequency-Detuned Grating Feedback

Song-Sui Li and Sze-Chun Chan, *Senior Member, IEEE*

***Abstract*—Chaotic dynamics of a semiconductor laser subject to optical feedback from a frequency-detuned fiber Bragg grating (FBG) is investigated experimentally and numerically. Although the FBG is similar to a mirror in perturbing the laser into chaos, it is not the same as a mirror because it provides spatially distributed reflections. Such distributed reflections effectively suppress the undesirable time-delay signature (TDS) contained in the autocorrelation function of the chaotic intensity time-series. The investigation shows that the best suppression of TDS is attained when the FBG is positively detuned from the free-running laser frequency. The TDS suppression is due to dispersion at frequencies near an edge of the main lobe of the FBG reflectivity spectrum. The suppression prefers the FBG at a positive detuning frequency because the laser cavity is red-shifted by the antiguidance effect. Numerically, the dynamical behavior is mapped in the parameter space of detuning frequency and feedback strength, where wide regions of chaos are identified. Experimentally, the TDS suppression by FBG feedback is demonstrated for the first time. The positively detuned FBG suppresses the TDS by over ten times to below 0.04 in the experiments.**

***Index Terms*—Optical chaos, time-delay signature, semiconductor laser, fiber Bragg grating.**

I. Introduction

SEMICONDUCTOR lasers subject to external feedbacks exhibit a wide range of interesting nonlinear dynamical behaviors [1]–[10]. A solitary single-mode semiconductor laser without feedback gives only continuous-wave (CW) emission, but it can be easily perturbed into different nonlinear dynamics which originate from the interactions between the intra-cavity optical fields and charge-carriers. The perturbation can be realized by different approaches such as optical injection and feedback [11]–[16], where the latter is one of the simplest approaches as it involves only one laser [17]–[19]. When a laser is subject to feedback, it manifests nonlinear behaviors including self-mixing [20], [21], low-frequency fluctuations [22], [23], intensity pulsations [9], [24], noise suppression [3], [25], [26], frequency oscillations [27]–[31], nonlinear transients [6], [7], and chaos [32]–[35]. The chaotic dynamics in semiconductor lasers with feedbacks are typically broadband, noise-like, synchronizable, and high-dimensional [36], [37]. These unique properties enabled a number of novel applications such as high-speed optical random bit generation [4], chaos-based secure communication [5], [18], and chaotic ranging [8], [24].

Despite being noise-like, the chaotic emission from a laser subject to feedback is prone to being scrutinized by some powerful nonlinear time-series analyses. Analyses using the permutation entropy, permutation statistical complexity, delayed mutual information (DMI), or autocorrelation function (ACF) on the laser emission intensity time-series allow the extraction of the information about the feedback delay time [38]–[44]. Similar analyses on the emission optical phase can further yield more information on the delay time [45]–[47]. Nonetheless, evaluating the ACF of the emission intensity time-series is the easiest approach towards time-delay identification [38], [39]. The approach is, for instance, readily affordable by an eavesdropper who attacks a chaos communication link. The residual peak in the ACF at the delay time is referred to as a time-delay signature (TDS). The TDS can clearly reveal the value of the delay time. Therefore, it was suggested that the TDS of the emission intensity ACF must be suppressed as much as possible [15], [48]–[51]. The TDS poses problems to the application of optical chaos. For example, it degrades the security in chaos communication, quality in random bit generation, and ambiguities in chaotic ranging applications [24], [52], [53].

Rontani *et al.* pioneered the suppression of TDS by optimizing the feedback strength in the simplest feedback configuration, which employs only one mirror [38], [39]. The numerical simulation showed a minimal TDS of about 0.15 by using an optimal feedback strength, which is sufficiently strong to induce chaos and yet not too strong to enhance TDS [38]. However, the approach usually requires relatively short feedback delay times, comparable to the period of the relaxation oscillation in order to obscure the TDS. Other different approaches to TDS suppression were subsequently reported by adopting more complicated configurations for feedbacks. These approaches include utilizing dual-path feedbacks using essentially two mirrors [35], mutually coupled feedbacks using two lasers [54], [55], feedback into a laser cascaded with injection into another laser [32], [49], and on-chip integrated optical feedback [50]. Interactions of different polarization modes in vertical cavity surface-emitting lasers (VCSELs) were also investigated in TDS suppression with mutual coupling, injection cascading, as well as polarization-preserved or polarization-rotated

Manuscript received February 2, 2015; revised April 23, 2015; accepted April 25, 2015. This work was supported by Grants from the Research Grant Council of Hong Kong, China (Project Nos. CityU 110712 and CityU 111213).

S.-S. Li is with the Department of Electronic Engineering, City University of Hong Kong, Hong Kong, China (e-mail: songsui.li@my.cityu.edu.hk).

S.-C. Chan is with the Department of Electronic Engineering, City University of Hong Kong, Hong Kong, China, and also with the State Key Laboratory of Millimeter Waves, City University of Hong Kong, Hong Kong, China (e-mail: scchan@cityu.edu.hk).

Color versions of one or more of the figures in this paper are available online at http://ieeexplore.ieee.org.

Digital Object Identifier 10.1109/JSTQE.2015.2427521

feedbacks [33], [56], [57]. These approaches to TDS suppression typically involved increasing the hardware complexity of the setup by adopting multiple lasers, multiple feedback loops, or multiple reflectors.

In order to simplify the constructions of these systems, an approach for TDS suppression by adopting a fiber Bragg grating (FBG) as the only reflector to a single-mode laser was proposed [51]. The approach was recently extended to VCSEL as well [58]. The approach employs an FBG as a distributed reflector in place of a single mirror, obscuring the round-trip feedback delay time, which leads to the reduction of the TDS. Comparing to other approaches of TDS suppression, the use of grating feedback is relatively simple as it only involves coupling light into an FBG. The approach is also a form of filtered optical feedback in which the filter spectral response is determined by the FBG. It complements some early investigations using feedbacks from idealized Lorentzian filters for some interesting frequency-dynamics and noise reduction effects [26]–[30]. Feedbacks from different practical gratings for wavelength stabilization have also been reported [31], [59], [60]. Nonetheless, the approach for suppressing TDS by FBG feedback was only numerically investigated [51], [58], where the effect of detuning the FBG from the laser have not been investigated numerically neither.

In this paper, TDS suppression of a single-mode semiconductor laser subject to feedback from an FBG is experimentally and numerically investigated. The numerical results first identify wide regions of chaotic dynamics over a range of FBG detuning frequency and feedback strength. Moreover, experimental results confirm the reduction of TDS when the FBG replaces a mirror for feeding back light into the laser. The reduction is attributed to the distributed reflections of the FBG, which correspond to the associated chromatic dispersion, according to numerical results. Furthermore, best suppression of the TDS is observed to occur when the FBG is positively detuned with respect to the free-running laser frequency. The feedback power causes red-shifting of the laser cavity through the antiguidance effect, pushing the emission towards the low frequency edge of the main lobe in the FBG reflectivity spectrum, which is associated with an enhanced dispersion for TDS suppression. With convenient adjustments of the detuning frequency, the experimental results show a minimal TDS of less than 0.04, which is below 10% of the original TDS from mirror feedback. The TDS is nearly perfectly concealed in the experiment using a positively detuned FBG feedback.

Following this introduction, the schematic and model of the laser with detuned FBG feedback are presented in Section II. The numerical results are described in Section III, while the experimental results are listed in Section IV. They are followed by a conclusion in Section V.

II. Setup

The setup for the experimental and numerical investigations is shown in Fig. 1. As illustrated by the schematic in Fig. 1(a), a single-mode semiconductor laser emits a linearly polarized light that is coupled through the lenses into a single-mode fiber

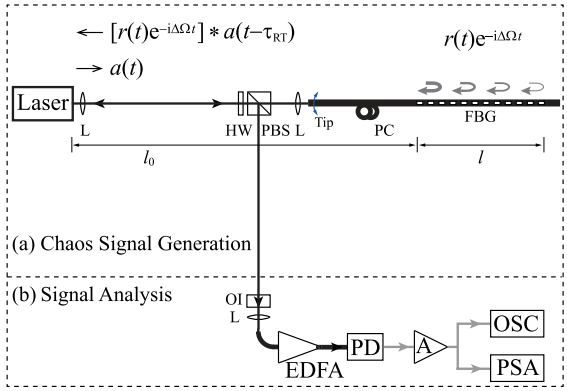

Fig. 1. (a) Schematic of chaos generation by a single-mode laser under feedback from a frequency-detuned grating for TDS suppression. The Bragg frequency of the grating is detuned by $\Delta f = \Delta\Omega/2\pi$ from the free-running optical frequency of the laser. (b) Setup for signal analysis. L: lens. HW: half-wave plate. PBS: polarizing beamsplitter. PC: polarization controller. FBG: fiber Bragg grating. OI: optical isolator. EDFA: erbium-doped fiber amplifier. PD: photodetector. A: microwave amplifier. PSA: power spectrum analyzer. OSC: oscilloscope. Thick lines: optical fibers. Thin lines: free-space optical paths. Gray lines: microwave cables.

appended with a FBG, which provides distributed reflections for optical feedback into the laser. A polarization controller is used to ensure that the polarizations entering into and reflecting from the fiber are equal, so that the power coupling back to the laser is maximized. The FBG is uniform and has no birefringence. The central frequency of its reflection spectrum, namely the Bragg frequency, is detuned by Δf from the free-running optical frequency of the laser. For example, a negative Δf means that the Bragg frequency is lower than the free-running frequency of the laser. The optical path length from the laser to the front-end of the FBG is denoted by l_0, which is longer than the physical length because of the refractive indices of the optical components such as the beamsplitter and the fiber. The corresponding feedback round-trip time is $\tau_{\mathrm{RT}} = 2l_0/c$ with c being the speed of light in vacuum.

Basically, as Fig. 1(a) shows, the chaos generation only requires coupling the laser and the FBG. Chaos is induced in the laser when the feedback strength is properly adjusted by the optical alignment of the fiber tip next to the lens. The TDS at τ_{RT} for the chaotic intensity ACF can be suppressed by optimizing the frequency detuning Δf. The combination of a half-wave plate and a polarizing beamsplitter is merely to split a small amount of the emitted light from the laser for signal analysis in Fig. 1(b). The emission is sent through a free-space optical isolator, focused by a lens into a fiber, and amplified by an erbium-doped fiber amplifier. A photodetector and a microwave amplifier then convert the optical intensity of the emission into an electrical signal for monitoring by a power spectrum analyzer and a real-time oscilloscope. Throughout the experiment, the half-wave plate is fixed for consistency. Single-mode fibers are used with angle-polished tips to avoid unwanted reflections feeding back to the laser.

The numerical simulation corresponding to the signal generation setup in Fig. 1(a) is based on modifying the Lang-Kobayashi model to incorporate the FBG [30], [38], [61]. The laser can

be described by the normalized intracavity optical field amplitude $a(t)$ and its normalized charge-carrier density $\tilde{n}(t)$. The field amplitude is a complex phasor quantity in reference to the free-running optical frequency of the laser. The rate equations governing the laser dynamics are [1], [51], [62], [63]

$$\frac{\mathrm{d}a}{\mathrm{d}t} = \frac{1-\mathrm{i}b}{2}\left[\frac{\gamma_\mathrm{c}\gamma_\mathrm{n}}{\gamma_\mathrm{s}\tilde{J}}\tilde{n} - \gamma_\mathrm{p}(|a|^2-1)\right]a + \gamma_\mathrm{c}\xi_\mathrm{f}e^{\mathrm{i}\theta}\left[r(t)e^{-\mathrm{i}\Delta\Omega t}\right] * a(t-\tau_\mathrm{RT}) \quad (1)$$

$$\frac{\mathrm{d}\tilde{n}}{\mathrm{d}t} = -(\gamma_\mathrm{s}+\gamma_\mathrm{n}|a|^2)\tilde{n} - \gamma_\mathrm{s}\tilde{J}\left(1-\frac{\gamma_\mathrm{p}}{\gamma_\mathrm{c}}|a|^2\right)(|a|^2-1) \quad (2)$$

where γ_c is the cavity decay rate, γ_s is the spontaneous carrier relaxation rate, γ_n is the differential carrier relaxation rate, γ_p is the nonlinear carrier relaxation rate, $\tilde{J}$ is the normalized bias current above threshold, and b is the linewidth enhancement factor for the antiguidance effect [25], [64]. These are the dynamical parameters within the laser itself, while the FBG feedback is described by the last term in (1). The term is proportional to the delayed optical field amplitude $a(t-\tau_\mathrm{RT})$ convoluted with $r(t)e^{-\mathrm{i}\Delta\Omega t}$. Here, $\Delta\Omega = 2\pi\Delta f$ is the angular frequency detuning of the Bragg frequency of the FBG away from the free-running frequency of the laser. $r(t)$ specifies the impulse response of the FBG with respect to the Bragg resonance frequency and so it equals the inverse Fourier transform of the reflection frequency response [29], [51], [58], [65]:

$$r(\Omega) = \Omega_\mathrm{BW} \times \left(2\Omega + \mathrm{i}\sqrt{\Omega_\mathrm{BW}^2 - 4\Omega^2}\coth\frac{\pi\sqrt{\Omega_\mathrm{BW}^2-4\Omega^2}}{2\Omega_l}\right)^{-1} \quad (3)$$

with FBG parameters $\Omega_\mathrm{BW} = 2\pi f_\mathrm{BW}$ and $\Omega_l = 2\pi f_l$. The full width at half-maximum (FWHM) reflection bandwidth of the main lobe is approximately f_BW for a highly reflective FBG, whereas the reciprocal of the round-trip propagation time inside the FBG is f_l. The peak reflectivity of $\tanh^2(\pi\Omega_\mathrm{BW}/2\Omega_l)$ is attained at the Bragg frequency of $\Omega = 0$. Once the FBG is selected, the feedback can still be adjusted by the grating detuning Δf and the normalized feedback strength ξ_f, which is proportional to the coupling efficiency between the laser and the fiber depending on the alignment of the fiber tip in Fig. 1(a) [51]. The feedback optical phase θ can in principle be adjusted by fine-tuning the optical path length from the laser to the grating corrugation. Based on the schematic in Fig. 1 on frequency-detuned FBG feedback, the numerical and experimental results on chaotic TDS suppression are detailed in the following sections.

III. Numerical Results

Numerical simulations are conducted based on (3) for the FBG as in Fig. 2 and the rate-equation model in (1)–(2) over a range of FBG detuning frequency Δf and feedback strength ξ_f in Fig. 3. Second-order Runge-Kutta integration is performed with time step and span of 2.38 ps and 1.25 μs, respectively. The results are obtained using the dynamical

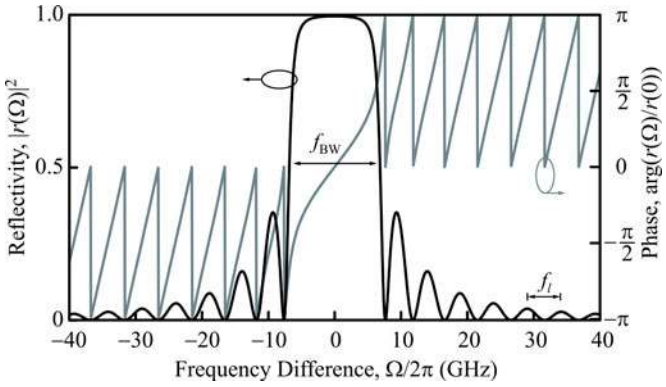

Fig. 2. FBG reflectivity spectrum $|r(\Omega)|^2$ (black) and phase spectrum $\arg(r(\Omega)/r(0))$ (gray). The frequency axis is centered at the Bragg frequency. The grating has a length of $l = 20$ mm for $f_l = 5$ GHz. Its FWHM bandwidth is $f_\mathrm{BW} = 13$ GHz.

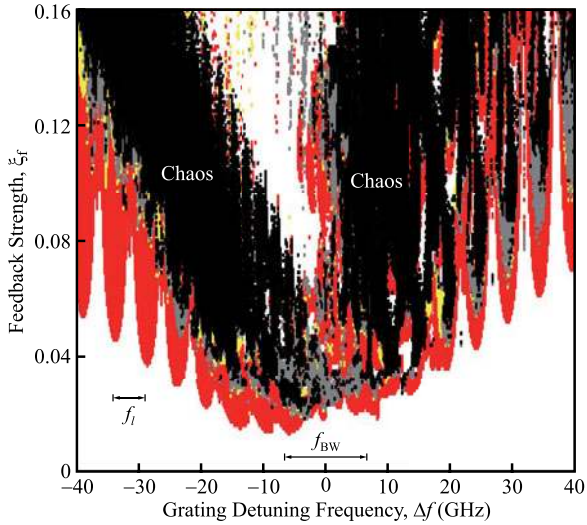

Fig. 3. Mapping of the output intensity dynamics in the parameter space of feedback strength ξ_f and grating detuning frequency Δf. The laser output intensity is stable (white), period-one oscillatory (red), quasi-periodic pulsating (gray), period-doubled oscillatory (yellow), and chaotic (black) in the different colored regions. The length of the FBG corresponds to $f_l = 5$ GHz. The bandwidth of the FBG is $f_\mathrm{BW} = 13$ GHz.

parameters previously extracted from a semiconductor laser with $\tilde{J} = 1.222$, $b = 3.2$, $\gamma_\mathrm{c} = 5.36\times10^{11}\mathrm{s}^{-1}$, $\gamma_\mathrm{s} = 5.96\times10^{9}\mathrm{s}^{-1}$, $\gamma_\mathrm{n} = 7.53\times10^{9}\mathrm{s}^{-1}$, and $\gamma_\mathrm{p} = 1.91\times10^{10}\mathrm{s}^{-1}$ [66]. Also, since the laser parameters correspond to a relaxation resonance frequency of $f_\mathrm{r} = 10.25$ GHz, a comparable grating bandwidth of $f_\mathrm{BW} = 13$ GHz is chosen for illustration [51]. In addition, $f_l = 5$ GHz is chosen throughout the simulations because it corresponds to a practical grating length of $l = 20$ mm with a refractive index of 1.5. The grating is chosen with θ set to zero. The numerical results focus on the case with a round-trip feedback delay time of $\tau_\mathrm{RT} = 0.47$ ns.

According to (3), the frequency response of the FBG reflection is plotted in Fig. 2. The reflectivity $|r(\Omega)|^2$ in black shows the main lobe of FWHM bandwidth f_BW and the associated side lobes, which peak with a periodicity of about f_l. The reflection phase $\arg(r(\Omega)/r(0))$ in gray shows rapid changes near the edges of the lobes. The changes correspond to

chromatic dispersion and have been well investigated for different gratings [65]. For the numerical integration of (1)–(2), the FBG frequency response $r(\Omega)$ is first inverse Fourier-transformed to the temporal impulse response $r(t)$, which vanishes for negative t as expected because of causality. Then, the convolution contained in the last term of (1) can be performed using the values of a previously obtained at and before $t - \tau_{\mathrm{RT}}$. It is worth noting that the magnitude of $r(t)$ is smaller than its peak value by more than 10^3 times when $t > 4$ ns, though $r(t)$ for a longer window of $0 < t < 10$ ns is adopted for improving accuracy in the numerical simulation.

In the feedback parameter space (ξ_{f}, Δf), Fig. 3 is a map of a number of regions for different output intensity dynamics. The dynamics are numerically identified through examining the distribution of the intensity time-series extrema [67]. The intensity is found as stable, period-one oscillatory, quasi-periodic pulsating, period-doubled oscillatory, and chaotic in the regions in white, red, gray, yellow, and black, respectively. Although there are interesting frequency-dynamics associated with systems with filtered optical feedback [27], [68], the following focuses on the intensity-dynamics as they can be most readily measured or eavesdropped in experiments [39]. Besides, no noise is included in the rate equations to avoid ambiguities in the boundaries of dynamical regions. Since the chaotic intensity variation is dominated by laser dynamics instead of noise, it is verified numerically that inclusion of spontaneous emission noise would not affect the chaotic TDS significantly [25].

Fig. 3 basically shows the quasi-periodic route-to-chaos for the laser with frequency-detuned FBG feedback. For instance, when ξ_{f} increases from zero at $\Delta f = \pm 24$ GHz, the intensity first remains stable in the white region, then oscillates periodically in the red region, pulsates quasi-periodically in a gray region, and finally behaves chaotically in a black region. Such a quasi-periodic route-to-chaos is commonly found in lasers subject to feedbacks [28], [67], [69]. Moreover, the minimum ξ_{f} required for instability roughly follows the inverse of the FBG reflectivity spectrum, which controls the power feeding back to the laser. For instance, when $|\Delta f| < f_{\mathrm{BW}}/2$, the free-running frequency of the laser is within the main lobe of the FBG reflection spectrum, so the instability requires only a feedback strength ξ_{f} of less than 0.02. But when $|\Delta f| \gg f_{\mathrm{BW}}$, the lower bound of the instability region is observed to undulate with a periodicity in Δf of about $f_l = 5$ GHz. The periodicity resembles that of the side lobes of the FBG reflection spectrum. A similar dependence of the stability boundary on the feedback reflection spectrum was also reported for Lorentzian filters [28]. Furthermore, a region of stability in white is observed at around (ξ_{f}, Δf) = (0.12, -8 GHz). The stable region is due to matching the FBG detuning frequency with the laser cavity resonance, which is red-shifted by the feedback through the antiguidance effect [28], [64], [70]. It is worth noting that the antiguidance effect also leads to asymmetry of the map with respect to the detuning, which is commonly observed for semiconductor laser dynamics [1], [64].

Most importantly, two large regions of chaotic operation are observed in the feedback parameter space (ξ_{f}, Δf), as labeled in Fig. 3. The regions are found with Δf being positive and negative, respectively. Since the setup in Fig. 1(a) is a time-delay system, information on the feedback delay time τ_{RT} could possibly be extracted from the waveforms. The rest of this work focuses on such time-delay information when the laser is in chaos.

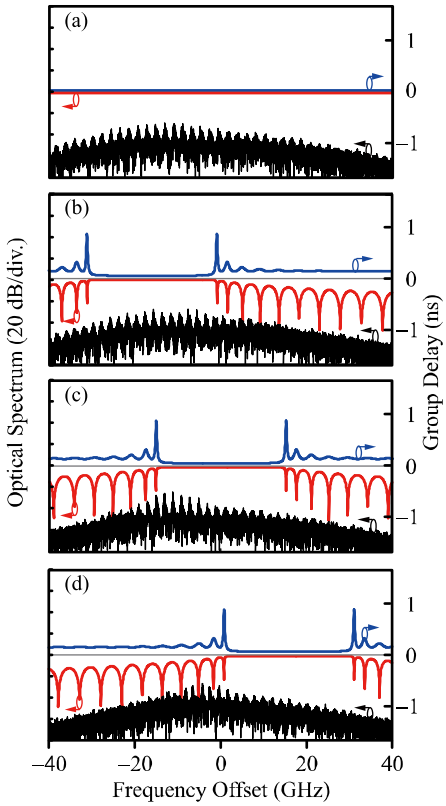

Fig. 4. Numerical results of the optical spectrum (black) for the chaotic laser emission. The laser is subject to feedback from (a) a mirror, (b) a negatively detuned FBG at $\Delta f = -16$ GHz, (c) a zero-detuned FBG at $\Delta f = 0$, and (d) a positively detuned FBG at $\Delta f = 16$ GHz, respectively. The frequency axis is offset to the free-running frequency of the laser. For reference, the optical reflectivity spectra of the mirror or the FBG are shown in red, whereas the corresponding group delays are shown in blue. The bandwidth of the FBG is $\Delta f = 28$ GHz.

A. *Chaotic Optical Spectrum*

Chaotic emissions for the laser subject to different optical feedbacks are compared in Fig. 4. Each black curve in Fig. 4(a)–(d) is a chaotic emission optical spectrum, namely, the Fourier transform of the field amplitude $a(t)$. The FBG bandwidth is chosen as $f_{\mathrm{BW}} = 28$ GHz for illustration in Fig. 4(b)–(d). The FBG is replaced by a conventional mirror for comparison in Fig. 4(a), which is modeled by setting $r(t)$ as the Dirac delta function $\delta(t)$ in (1). The feedback strength is fixed at $\xi_{\mathrm{f}} = 0.078$ while the feedback delay time is kept at $\tau_{\mathrm{RT}} = 0.47$ ns. The frequency axis is offset to the free-running frequency of the laser. For reference in Fig. 4, the red and blue curves respectively show the magnitude and group delay associated with the frequency response $r(\Omega - \Delta\Omega)$ of the feedback.

Starting with Fig. 4(a), the FBG is first replaced by a conventional mirror for comparison. The reflectivity spectrum in red is just a flat line as the mirror has no frequency-selectivity. The group delay spectrum in blue is simply zero because the mirror itself does not induce any delay. The optical feedback is

sufficiently strong in perturbing the laser into chaos. The broadband optical spectrum in black spans a frequency range of over 10 GHz [71]. The bandwidth is comparable to the relaxation resonance frequency as in most cases of semiconductor laser chaos [71]. Also, the optical feedback power into the laser reduces the optical gain, which red-shifts the cavity resonance frequency through the refractive index change by the antiguidance effect [64], [72]. The red-shift is apparent from the enhanced peaks at negative frequency offset in Fig. 4(a). However, the broadband spectrum clearly consists of periodic peaks separated by about 2 GHz which roughly corresponds to $1/\tau_{\mathrm{RT}}$. The peaks can be interpreted as the external cavity mode structures. Such spectral features could undesirably reveal the time-delay information. In order to better conceal the time-delay information, the FBG is adopted in lieu of the mirror for providing distributed feedback in Fig. 4(b)–(d).

In Fig. 4(b), the FBG is negatively detuned by setting $\Delta f = -16$ GHz. The red curve shows the FBG reflectivity spectrum that is centered at the frequency offset of -16 GHz. The FBG is a uniform grating so that its main lobe has a bandwidth of about $f_{\mathrm{BW}} = 28$ GHz and its side lobes are roughly separated by $f_l = 5$ GHz [65]. The blue curve shows the group delay associated with the FBG. The delay is obtained from the phase of FBG frequency response. Nonetheless, the laser still experiences the antiguidance effect, so that its peak emission continues to be red-shifted from its free-running frequency, as the spectrum in black shows. Most of the emitted power is contained within the main lobe of the FBG reflectivity spectrum, which is quite flat and does not involve much group delay. Therefore, the chaotic spectrum still contains clear external cavity mode structures separated by $1/\tau_{\mathrm{RT}}$.

In Fig. 4(c), the FBG is not detuned as Δf is set at 0. The FBG reflectivity spectrum in red is now centered at the free-running frequency of the laser, while the group delay in blue is also centered accordingly. Such a zero-detuned FBG feedback has been investigated previously through optimizing the grating design parameters such as its bandwidth and physical length, which led to better concealment of the time-delay information as compared to mirror feedback [37], [51]. Nonetheless, with the FBG in Fig. 4(c), the optical spectrum in black still contains some external cavity mode structures separated by $1/\tau_{\mathrm{RT}}$. The emission power is now spread across the main lobe and some side lobes at negative frequencies.

Finally, in Fig. 4(d), when the FBG is positively detuned at $\Delta f = 16$ GHz. The FBG reflectivity spectrum in red is centered at a higher frequency than the laser free-running frequency. As the black curve shows, the optical spectrum of the laser emission again peaks at red-shifted frequencies. The strongest emission peaks are now mainly found in the low frequency side lobes. Interestingly, as the blue curve shows, the group delay has much variation near the edge of the main lobe and its neighboring side lobes. The frequency-dependent group delay, corresponding to the group velocity dispersion, of the FBG feedback obscures the information on the round-trip time delay. A direct comparison of Fig. 4(a) and (d) confirms that the external mode structures are more pronounced for mirror feedback than for FBG feedback. Therefore, a positively detuned FBG is effective in concealing the information of τ_{RT}. The improvement can be quantified by the so-called coherence function from the inverse Fourier transform on the magnitude of the optical spectra. The magnitude of the normalized coherence function at τ_{RT} drops from 0.5 in Fig. 4(a) to 0.3 in Fig. 4(d).

B. Suppression of TDS

The above qualitatively illustrates the effect of frequency-detuned FBG feedback by examining the optical spectrum. The side-lobe group delay variation of the detuned FBG moderately weakens the structures in the optical spectrum that contain the time-delay information. Nonetheless, while there are interesting reports on the information contained in the optical phase [46], [47], [52], most related studies focus on the time-delay information contained in the intensity time-series [15], [34], [39], [57]. For many applications of laser chaos such as chaotic ranging and random bit generation, the practical performances are degraded if the intensity time-series partially repeats itself after a delay [24], [53], [73]. Such a correlation is revealed by examining the ACF, as Fig. 5 illustrates.

Fig. 5(a)–(d) plot the power spectra, intensity time-series, as well as the ACF and DMI of the intensity time-series, which correspond to the optical spectra in Fig. 4(a)–(d). Column (ii) of Fig. 5 shows the intensity time-series $I(t) = |a(t)|^2$. Column (i) shows the power spectra by Fourier-transforming $I(t)$, while column (iii) shows the autocorrelation of $I(t)$ as a function of the lag time τ. Column (iv) shows, as a function of lag time τ, the mutual information between the intensity time-series $I(t)$ and its delayed replica $I_\tau(t) = I(t-\tau)$ [38]. Such a DMI is defined as the sum of $p(I, I_\tau)\log[p(I, I_\tau)/(p(I)p(I_\tau))]$ over the two-dimensional space (I, I_τ), where $p(I)$ is the probability density function of I and $p(I, I_\tau)$ is the joint probability density function of (I, I_τ). Each DMI curve in Fig. 5 is normalized to its value at zero τ when I and I_τ are the same. For the plots in Fig. 5, the bandwidth of the FBG is kept at $f_{\mathrm{BW}} = 28$ GHz. The round-trip feedback delay time is set at $\tau_{\mathrm{RT}} = 0.47$ ns.

Starting with Fig. 5(a), the laser is perturbed into chaos by a mirror feedback. Its power spectrum Fig. 5(a-i) is broadband and peaks at around the relaxation resonance frequency f_{r} of about 10.25 GHz. The behavior is typical of semiconductor laser chaos due to the undamping of the relaxation resonance [74]. The external cavity mode structures Fig. 4(a) lead to multiple peaks in the power spectrum of Fig. 5(a-i), where the separation of about 2 GHz again corresponds to the reciprocal of τ_{RT}. The corresponding time-domain waveform in Fig. 5(a-ii) is noise-like without much recognizable features because of the broadband power spectrum. However, the ACF in Fig. 5(a-iii) is found to contain observable peaks when the lag time τ equals any multiples of the feedback delay time τ_{RT}. The peak at $\tau = \tau_{\mathrm{RT}}$ is referred to as the TDS [32], [35], [38]. The TDS is about 0.4 on the ACF. The TDS is relatively large because the mirror gives a constant feedback delay time independent of the optical frequency. Besides, oscillations on the order of 0.1 ns are observed around the peaks of the ACF. These oscillations correspond to the reciprocal of f_{r} due to the enhancement of the power spectrum near the relaxation resonance [39]. Consistent

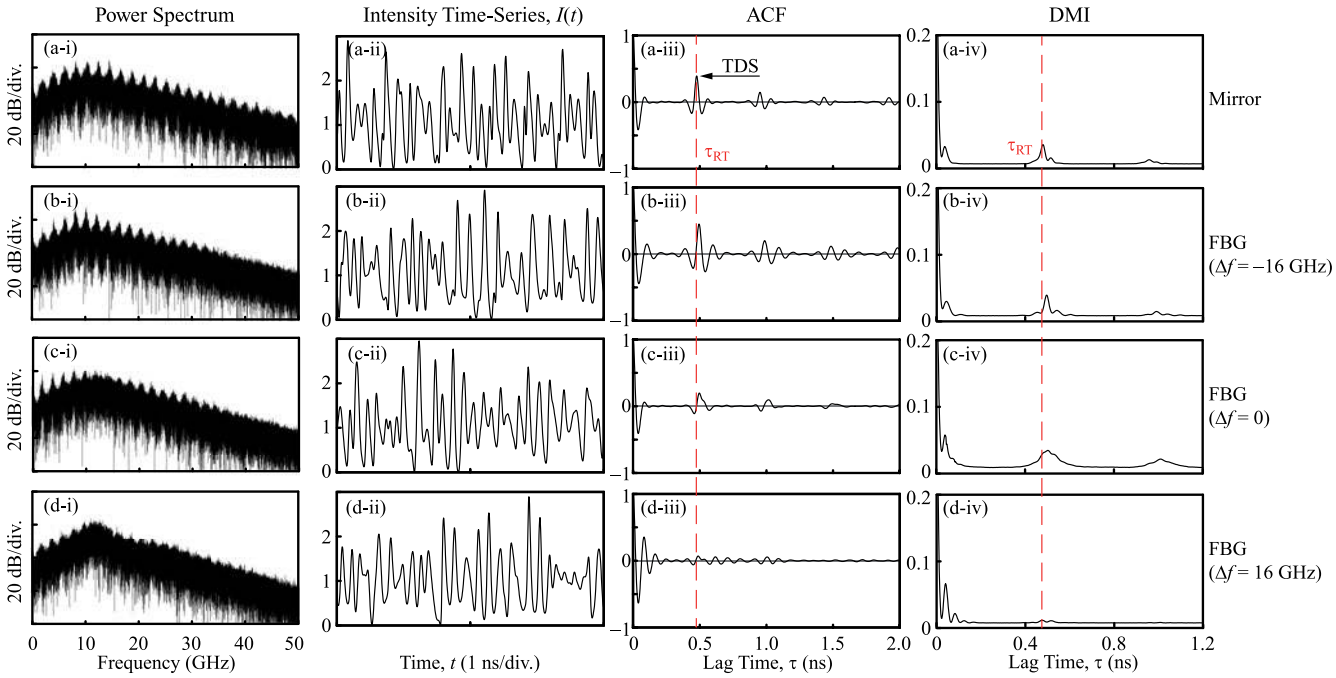

Fig. 5. Numerical results of the laser emission (i) power spectrum, (ii) intensity time-series, (iii) ACF of the intensity time-series, and (iv) DMI of the intensity time-series. The laser is subject to feedback from (a) a mirror, (b) a negatively detuned FBG at $\Delta f = -16$ GHz, (c) a zero-detuned FBG at $\Delta f = 0$, and (d) a positively detuned FBG at $\Delta f = 16$ GHz, respectively. The bandwidth of the FBG is $f_{\mathrm{BW}} = 28$ GHz. The round-trip feedback delay time between the laser and the grating is $\tau_{\mathrm{RT}} = 0.47$ ns.

with the ACF, the DMI in Fig. 5(a-iv) also shows a clear peak at $\tau = \tau_{\mathrm{RT}}$.

In Fig. 5(b), the FBG is negatively detuned by setting $\Delta f = -16$ GHz. With the replacement of the mirror by the FBG, the chaotic time-series in Fig. 5(b-ii) does not show much changes. The power spectrum in Fig. 5(b-i) still peaks at around f_{r} without much modification on the structures separated by 2 GHz. This is consistent with the fact that the optical spectrum in Fig. 4(b) is not much modified by replacing the mirror with a negatively detuned FBG. Therefore, the ACF still contains a clear TDS at $\tau_{\mathrm{RT}} = 0.47$ ns as shown in Fig. 5(b-iii), where the DMI also peaks at τ_{RT} in Fig. 5(b-iv).

In Fig. 5(c), when the FBG is not detuned as Δf is set at zero. The time-series in Fig. 5(c-ii) remains chaotic. The power spectrum Fig. 5(c-i) still peaks near f_{r}, but the structures separated by 2 GHz become less observable. This is attributed to the group-delay dispersion near the low frequency edge of the main lobe and the lower side lobes of the FBG, as the optical spectrum in Fig. 4(c) suggests. Quantitatively, the ACF in Fig. 5(c-iii) has a reduced TDS of 0.18 at τ_{RT}. The zero-detuned FBG feedback suppresses the TDS as compared to mirror feedback. The DMI peak in Fig. 5(c-iv) at the vicinity of τ_{RT} is also broadened in obscuring the time-delay information. Detailed optimization of the grating design was previously investigated numerically without detuning [51].

The suppression of TDS continues in Fig. 5(d) when the FBG is positively detuned at $\Delta f = 16$ GHz. The power spectrum Fig. 5(d-i) becomes much smoother when compared to Fig. 5(a-i). This is again consistent with the observation of the corresponding optical spectrum in Fig. 4(d), which contains less pronounced peaks as compared to Fig. 4(a). The time-series is again chaotic in Fig. 5(d-ii). The corresponding ACF in Fig. 5(d-iii) clearly shows a suppression of TDS to less than 0.07. Moreover, the DMI in Fig. 5(d-iv) also contains nearly no peaks near τ_{RT}. Thus, the delay time τ_{RT}, as marked by the dashed lines in Fig. 5(d-iii) and (d-iv), cannot be easily extracted even with the knowledge of ACF and DMI.

In short, the detuning frequency Δf of the FBG is an important parameter that affects the TDS. Best suppression of TDS is achieved when the FBG is positively detuned. The positive detuning forces the laser to emit near the low frequency edge of the main lobe and the nearby side lobes. They provide relatively strong chromatic dispersion of the group delay for TDS suppression.

C. *Dependence on* $(\xi_{\mathrm{f}}, \Delta f)$

While the grating design parameters such as its length and bandwidth are relatively difficult to adjust in experiments, the detuning frequency of the FBG with respect to the free-running frequency of the laser is more easily adjusted, as Section IV details. The dependence of the properties of the chaotic signal on the detuning frequency Δf are presented in Fig. 6. The TDS in the ACF of the intensity is shown in row (a). The chaotic bandwidth (CBW) is shown in row (b). The CBW is the effective bandwidth that contains 80% of the total power in the chaotic power spectrum, as defined in previous works on laser chaos [71]. Different columns in Fig. 6 correspond to different grating bandwidths f_{BW} as labeled. The feedback strengths are kept at $\xi_{\mathrm{f}} = 0.078$, 0.10, and 0.12 for the circles, squares, and

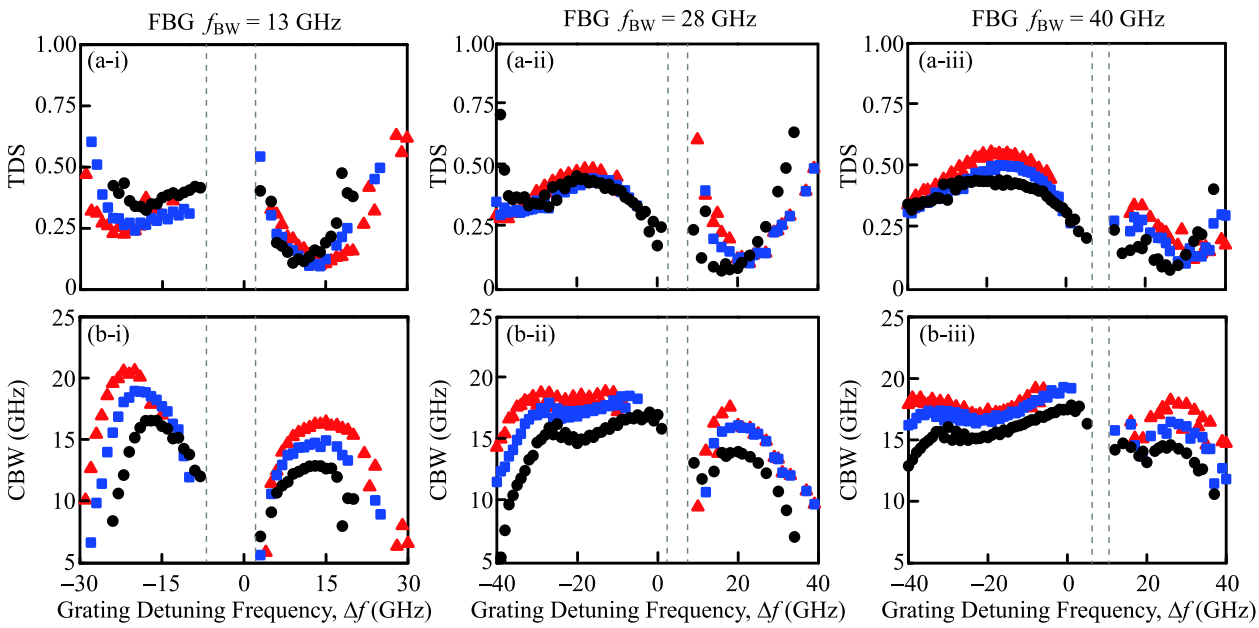

Fig. 6. Numerical results of (a) TDS and (b) effective bandwidth for the chaotic signals as functions of the FBG detuning frequency Δf. The feedback strength is fixed at $\xi_f = 0.078$ (circles), 0.10 (squares), and 0.12 (triangles), respectively. The FBG bandwidth f_{BW} = (i) 13 GHz, (ii) 28 GHz, and (iii) 40 GHz, respectively.

triangles, respectively. For each plot, the gap of Δf bounded by the dashed lines indicates a region without chaotic intensity oscillation. The gap in Fig. 6(a), for example, roughly corresponds to the white region of intensity-stability in between the two chaotic region labeled in the map of Fig. 3. Since the stable white region is attributed to the filtered feedback stabilization for CW emission [28], [70], the gap becomes narrowed as the FBG becomes less frequency-selective. Narrowing of the gap between the dashed lines is observed in Fig. 6(a), (b), and (c) when the FBG bandwidth f_{BW} is increased progressively at 13, 28, and 40 GHz, respectively. The gap vanishes eventually when the f_{BW} goes to infinity as the FBG simply becomes a mirror. For Fig. 6(b-i)–(b-iii), the CBW is shown to increase as the detuning frequency leaves the gaps. The CBW is on the order of the relaxation resonance frequency f_r as in most chaotic lasers [71]. Comparing the circles, squares, and triangles also shows a general increment of CBW as the feedback strength increases, which is linked to the bandwidth enhancement effect in the semiconductor laser [16]. As for TDS, Fig. 6(a-i)–(a-iii) clearly shows the dependence on Δf. The variation of the TDS with respect to Δf is basically the reverse of that for CBW, as both TDS and CBW quantify the chaotic signals. Most interestingly, the lowest TDS in each plot is always attained when $\Delta f > 0$. With $\xi_f = 0.078$, the minimal TDS of 0.07 is attained in Fig. 6(a-ii) for a positively detuned FBG of $\Delta f = 16$ GHz which corresponds to Fig. 5(d-iii). The results in Fig. 6 confirm the advantage of adopting a positively detuned FBG for TDS suppression.

In addition to the detuning frequency Δf, the feedback strength ξ_f can also be adjusted conveniently in experiments. TDS and CBW are respectively shown against the feedback strength in Fig. 7(a) and (b) when the laser is in chaos. The FBG bandwidth is fixed at $f_{BW} = 13$ GHz (closed down-triangles),

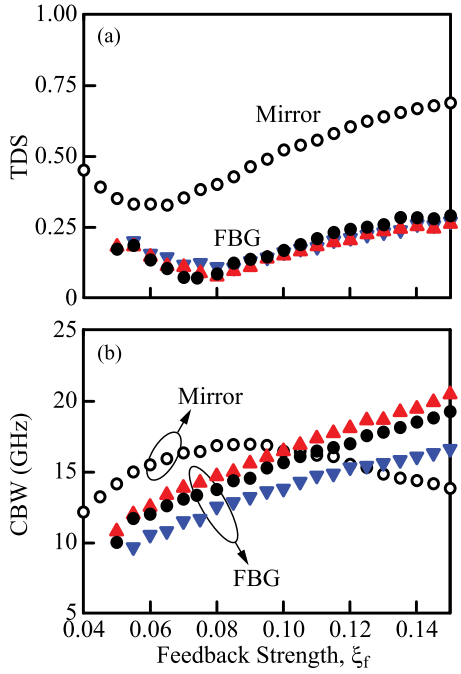

Fig. 7. Numerical results of (a) TDS and (b) effective bandwidth for the chaotic signals as functions of the feedback strength ξ_f. FBGs of bandwidths $f_{BW} = 13$ GHz, 28 GHz, and 40 GHz are considered in closed down-triangles, closed circles, and closed up-triangles, respectively. For comparison, the open circles are obtained when the FBG is replaced by a mirror.

28 GHz (closed circles), and 40 GHz (closed up-triangles), where the detuning is kept at $\Delta f = 9$ GHz, 16 GHz, and 27 GHz, respectively. For each f_{BW}, the values of Δf are chosen to minimize the TDS at $\xi_f = 0.078$ by referencing to Fig. 6. For comparison, a mirror replaces the grating for the

results in open circles. In Fig. 7(a), independent of the grating or the mirror, TDS is found to first reduce and then increase as $\xi_{\rm f}$ increases. Such a dependence of TDS on $\xi_{\rm f}$ has been reported before for mirror feedback, which is related to having sufficient feedback power to perturb the laser into chaos while not inducing much external cavity features from the feedback [38]. It is clear from Fig. 7(a) that the FBGs are better than the mirror for TDS suppression. In Fig. 7(b), the CBW generally broadens as $\xi_{\rm f}$ increases from zero. This is due to the evolution of the laser from stability into chaos. When the $\xi_{\rm f}$ increases beyond about 0.08, the CBW from mirror feedback starts to saturate and even gradually reduce. This is not observed for the three cases of FBG feedbacks, but it should be mentioned that strong feedbacks can occasionally drive the laser back to stability as the map in Fig. 3 shows.

In any cases, it is clear from Fig. 7(b) that the CBW from the positively detuned FBG feedbacks are comparable to that for mirror feedback. By using a positively detuned FBG in place of a mirror for feedback, the TDS can be reduced while maintaining the same CBW.

IV. Experimental Results

Experimental verification on the TDS suppression by FBG feedback has not been reported so far, to our best knowledge, on semiconductor lasers with or without frequency detuning. In this section, an experimental investigation on TDS suppression by optical feedback from an FBG is conducted based on the setup in Fig. 1. In Fig. 1(a), optical feedback from the FBG is implemented for chaos generation in a 1548-nm single-mode distributed-feedback laser (Mitsubishi ML920T43S-01). The laser is temperature-stabilized at 17.8 °C and forward-biased at 13 mA, which corresponds to 1.3 times its threshold current. It outputs about 2.3 mW with relaxation resonance frequency $f_{\rm r} \approx 5$ GHz. A commercially available FBG with a Bragg wavelength also at 1548 nm is adopted. It has a 3-dB bandwidth of 0.45 nm or, equivalently, $\Delta f = 56$ GHz. It is a uniform grating formed by corrugations written over a physical length of $l = 8$ mm on the fiber with a refractive index $n = 1.45$ so that $f_l = c/2nl \approx 13$ GHz. The peak reflectivity is confirmed as higher than -1 dB from direct experimental calibration. The setup of Fig. 1 is constructed with the laser and the fiber tip being separated by only 0.24 m, but there is also about 4.17 m of single-mode fiber with a group index of 1.47 before reaching the FBG. The corresponding optical path of $l_0 = 6.37$ m gives the external cavity round-trip time of $\tau_{\rm RT} = 42.5$ ns.

The feedback strength $\xi_{\rm f}$ is controlled by carefully adjusting the misalignment of the fiber tip. It is proportional to the coupling efficiency from the laser into the fiber, where the proportionality constant approaches 0.5 for a high-quality laser cavity [74], [75]. Also, for analyzing the signal using the setup in Fig. 1(b), the beamsplitter directs less than 10% power to the optical amplifier of 10-dB gain (Amonics AEDFA-23-B-FA), then the photodetector (Newport AD-10ir), and the 20-dB microwave amplifier (HP 83006 A). The output electrical signal, proportional to the intensity of the laser emission, is monitored in the time-domain by the real-time oscilloscope of 2.5-GHz bandwidth (Agilent 90254A) and in the frequency-domain by the power spectrum analyzer of 26.5-GHz bandwidth (Agilent N9010A). In the experiments, the detuning frequency Δf is adjusted by varying the laser free-running frequency through temperature-tuning. The detuning frequency Δf changes by about 13 GHz/°C when the FBG is kept unchanged. The following discusses the experimental results on TDS suppression.

A. Suppression of TDS

Fig. 8 shows the experimental data that confirm the TDS suppression. The laser is under FBG feedback with a negative detuning at $\Delta f = -40$ GHz, zero detuning at $\Delta f = 0$, and positive detuning at $\Delta f = 40$ GHz as shown in Fig. 8(b)–(d), respectively. The FBG is replaced by a mirror for comparison in Fig. 8(a). The feedback strength is kept at $\xi_{\rm f} = 0.06$. The power spectra in column (i) are shown with the full frequency-span of the power spectrum analyzer at a resolution bandwidth of 2.6 MHz. The power spectra are similar in having an enhancement at around the relaxation resonance frequency of $f_{\rm r} \approx 5$ GHz. Such an enhancement is typical of chaotic signals in semiconductor lasers [12].

To show the spectra in detail, the insets in column (i) plot the power spectra by zooming to a reduced span of 200-MHz around the peak frequency of 5 GHz with a resolution of 25 kHz. With mirror feedback in Fig. 8(a-i) inset, the spectrum shows a clear and repeating feature in every 24 MHz, which corresponds to $1/\tau_{\rm RT}$. With FBG feedbacks in Fig. 8(b-i)–(c-i) insets, the repeating features become less apparent. Interestingly, by detuning the FBG feedback positively, the repeating feature vanishes completely in the inset of Fig. 8(d-i). The positive detuning of $\Delta f = 40$ GHz puts the laser close to the low frequency edge of the FBG main lobe, which results in the elimination of any repeating feature for Fig. 8(d-i).

As for the time-domain, column (ii) in Fig. 8 shows the intensity recorded by the oscilloscope. It should be pointed out that the oscilloscope has a limited bandwidth of 2.5 GHz, so the faster oscillations of the chaotic signals are not recorded directly. However, the intensity time-series sufficiently confirms the random-like property of chaotic signals. The time-delay information of the setup is not apparent in the time-series, as in the case of numerical simulations in column (ii) of Fig. 5. The ACF can be obtained by directly correlating the time-series, but it can also be calculated by taking inverse Fourier transform on the power spectrum. The latter approach, as supported by the Wiener-Khinchin theorem, avoids the bandwidth limitation of the oscilloscope. The ACFs in Fig. 8(a-iii)–(d-iii) are obtained by transforming the power spectra recorded in Fig. 8(a-i)–(d-i), respectively. For Fig. 8(a-iii), the ACF produces a pronounced peak at $\tau_{\rm RT} = 42.5$ ns, as marked by the red arrow. The strong TDS is nearly 0.5 for the mirror feedback chaos, which corresponds to the pronounced repeating spectral features in Fig. 8 (a-i) inset. For Fig. 8(b-iii), the TDS is slightly reduced by the FBG feedback with negative detuning. It further subsides when the FBG has no detuning in Fig. 8(c-iii). Finally, in Fig. 8(d-iii), the TDS basically disappears in the ACF. There is nearly no peaks observed at $\tau_{\rm RT}$, as indicated by the red arrow, except

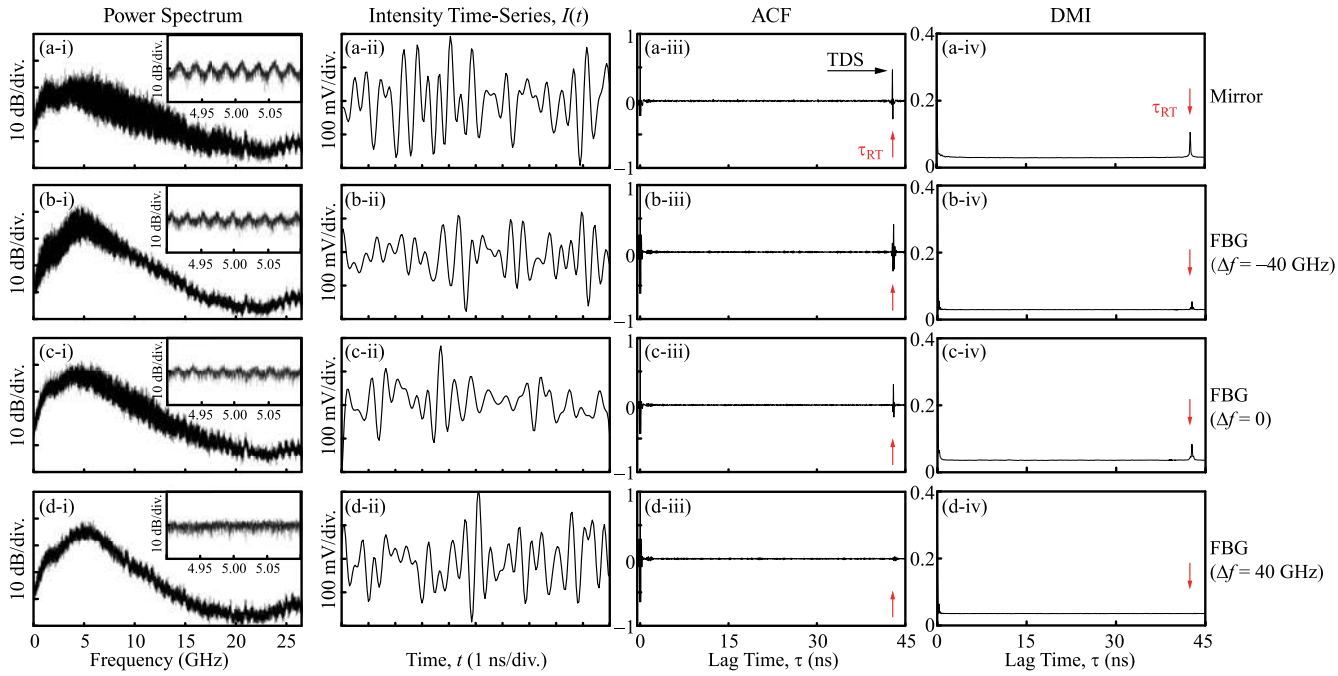

Fig. 8. Experimental results of the laser emission (i) power spectrum in full span (with inset zoomed to a 200-MHz span), (ii) intensity time-series, (iii) ACF of the intensity time-series, and (iv) DMI of the intensity time-series. The laser is subject to feedback from (a) a mirror, (b) a negatively detuned FBG at $\Delta f = -40$ GHz, (c) a zero-detuned FBG at $\Delta f = 0$, and (d) a positively detuned FBG at $\Delta f = 40$ GHz, respectively. The bandwidth of the FBG is $f_{\mathrm{BW}} = 56$ GHz. The round-trip feedback delay time between the laser and the grating is $\tau_{\mathrm{RT}} = 42.5$ ns.

for a very small residual TDS of less than 0.04. The TDS is suppressed by over 10 times when compared to using mirror feedback. Hence, the experiment confirms the numerical results on chaotic TDS suppression by a positively detuned FBG feedback.

In addition, the DMI is evaluated in column (iv) of Fig. 8 based on the intensity time-series of column (ii) over a time span of 5 μs. Mirror feedback in Fig. 8(a-iv) again shows a pronounced DMI peak at $\tau_{\mathrm{RT}} = 42.5$ ns as the red arrow indicates. Replacing the mirror by the FBG in Fig. 8(b-iv)–(d-iv) again gives significant suppression of the peak. For the positively detuned FBG feedback, Fig. 8(d-iv) unveils no DMI peak near τ_{RT}, thus confirming the concealment of the time-delay information.

B. Dependence on $(\xi_{\mathrm{f}}, \Delta f)$

By adjusting the temperature of the laser, its free-running emission frequency is varied, thus the detuning frequency Δf of the fixed FBG is modified. The closed symbols in Fig. 9 show the TDS and CBW from the experiments as Δf varies, where the feedback strength is kept at 0.06. A gap in between the dashed line again represents a range of Δf without chaotic signals. Other than the gap, the chaotic signal maintains a wide bandwidth according to Fig. 9(b). The CBW is roughly the same as the relaxation resonance frequency f_{r} of 5 GHz. As for TDS of the ACF, Fig. 9(a) shows its dependence against the detuning. Best suppression is obtained at a positive detuning of $\Delta f = 40$ GHz, where the TDS is less than 0.04 as in Fig. 8(d-iii).

Moreover, as the temperature-tuning may also affect the dynamical parameters of the laser, it is necessary to compare the

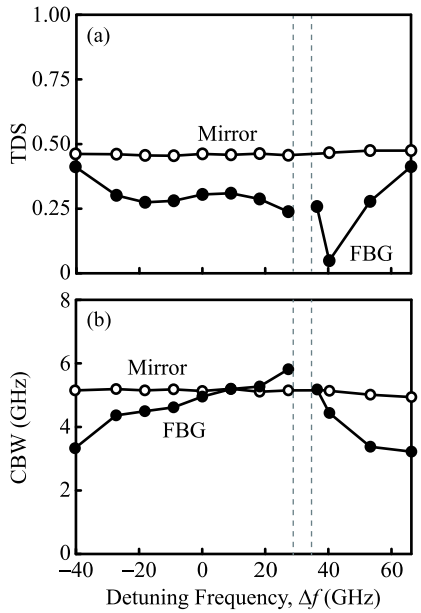

Fig. 9. Experimental results in closed symbols for (a) TDS and (b) effective bandwidth for the chaotic signals as functions of the FBG detuning frequency Δf, as varied by adjusting the free-running laser frequency. The FBG has a bandwidth of $f_{\mathrm{BW}} = 56$ GHz. For comparison, the open symbols are obtained when the FBG is replaced by a mirror. The feedback strength is fixed at $\xi_{\mathrm{f}} = 0.06$.

FBG feedback with mirror feedback at the same laser temperature. So the data in open symbols in Fig. 9 are obtained for mirror feedback. The axis on detuning is still representing the difference of the fixed Bragg frequency from the free-running laser frequency, though the FBG is not connected to the experimental

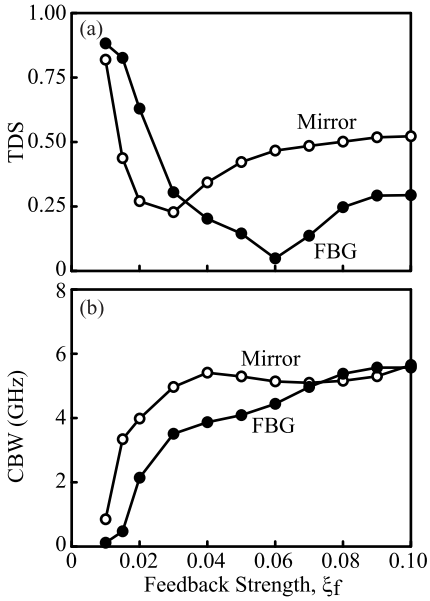

Fig. 10. Experimental results in closed symbols of (a) TDS and (b) effective bandwidth for the chaotic signals as functions of the feedback strength $\xi_{\rm f}$. The FBG bandwidth is $f_{\rm BW} = 56$ GHz. For comparison, the open symbols are obtained when the FBG is replaced by a mirror.

setup for the open symbols. In other words, any two vertically separated closed and open symbols in Fig. 9 are recorded for the same laser temperature. The results of the mirror feedback show that both the TDS and CBW do not change much even when the laser temperature is tuned. On TDS suppression, FBG feedback consistently outperforms mirror feedback.

For completeness, the feedback strength $\xi_{\rm f}$ is varied in Fig. 10 by fine-adjusting the optical misalignment of the fiber tip in Fig. 1(a). The laser temperature is kept constant so that Δf stays at 40 GHz. Fig. 10(a) shows the TDS first drops and then increases as $\xi_{\rm f}$ is increased. Such a dependence is consistent with the reports on mirror feedback [38], [39]. FBG feedback (closed symbols) again shows lower TDS as compared to mirror feedback (open symbols). The minimum TDS for FBG feedback is attained at $\xi_{\rm f} = 0.06$. It is interesting that the minimum TDS for mirror feedback is attained at a smaller $\xi_{\rm f}$ of 0.03. Thus, the optimal $\xi_{\rm f}$ for TDS suppression is increased when the mirror is replaced by the FBG. The increment is also observed in the numerical simulation in Fig. 7(a). Such an increment is expected from (1) because the feedback field is proportional to not only $\xi_{\rm f}$, but also $r(t)$ when incorporating the FBG. While the optical coupling between the laser and the fiber in Fig. 1(a) is quantified by $\xi_{\rm f}$, the reflectivity by the FBG is quantified by $r(t)$ and in turn $r(\Omega)$ according to (3). Due to the detuning of $\Delta f =$ 40 GHz, the laser emission is not within the FBG main lobe of near perfect reflectivity, but is rather situated in a side lobe with only about 0.3 reflectivity. As a result, $\xi_{\rm f}$ needs to be increased for optimal TDS suppression when using the FBG.

In addition, Fig. 10(b) shows the CBW that grows with the feedback strength. There is only a slight difference in bandwidth between mirror feedback (open symbols) and FBG feedback (closed symbols). Therefore, FBG feedback is experimentally demonstrated as a simple approach to achieve TDS suppression, where a positive detuning frequency of the grating from the laser is preferred. The experimental results in Figs. 8–10 also agree qualitatively with the numerical results in Figs. 5–7. At this point, a quantitative performance comparison of FBG feedback is drawn with some other TDS suppression approaches. These approaches typically involved more complicated construction such as double optical feedback using two precisely located mirrors [35], mutual coupling using two lasers [55], and cascaded coupling using even three lasers [49]. The reported experimental values of the TDS in ACF of these approaches were no less than 0.04. By contrast, FBG feedback investigated in this paper gives a suppressed TDS of 0.04, but it is structurally much simpler than the other approaches, as it uses only one laser with a fiber grating.

V. Conclusion

In summary, evolution of the TDS in the ACF of the chaotic intensity time-series is investigated on a single-mode semiconductor laser subject to feedback of a frequency-detuned FBG. Suppression of TDS by a positively detuned FBG is experimentally demonstrated. Numerically, a dynamical map revealing large regions of chaotic operation is reported in the parameter space of $(\xi_{\rm f}, \Delta f)$. TDS suppression prefers adopting FBG feedback over mirror feedback. It also prefers a positive detuning over a negative detuning. Experimentally, as compared to mirror feedback, TDS is suppressed by 10 times to less than 0.04 when using a positively detuned uniform FBG for the feedback. The approach is relatively simple in the experimental setup, which implies its potentials in applications relying on semiconductor laser chaos.

References

[1] S. Donati and R. H. Horng, "The diagram of feedback regimes revisited," *IEEE J. Sel. Topics Quantum Electron.*, vol. 19, no. 4, p. 1500309, Jul./Aug. 2013.

[2] M. Sciamanna and K. A. Shore, "Physics and applications of laser diode chaos," *Nat. Photon.*, vol. 9, pp. 151–162, 2015.

[3] T. B. Simpson, J. M. Liu, M. AlMulla, N. G. Usechak, and V. Kovanis, "Linewidth sharpening via polarization-rotated feedback in optically injected semiconductor laser oscillators," *IEEE J. Sel. Topics Quantum Electron.*, vol. 19, no. 4, p. 1500807, Jul./Aug. 2013.

[4] A. Uchida *et al.*, "Fast physical random bit generation with chaotic semiconductor lasers," *Nat. Photon.*, vol. 2, pp. 728–732, Dec. 2008.

[5] A. Argyris *et al.*, "Chaos-based communications at high bit rates using commercial fibre-optic links," *Nature*, vol. 438, pp. 343–346, Nov. 2005.

[6] D. Brunner, M. C. Soriano, C. R. Mirasso, and I. Fischer, "Parallel photonic information processing at gigabyte per second data rates using transient states," *Nat. Commun.*, vol. 4, pp. 1364-1–1364-7, Jan. 2013.

[7] M. C. Soriano, J. Garcia-Ojalvo, C. R. Mirasso, and I. Fischer, "Complex photonics: Dynamics and applications of delay-coupled semiconductors lasers," *Rev. Mod. Phys.*, vol. 85, pp. 421–470, Mar. 2013.

[8] F. Y. Lin and J. M. Liu, "Diverse waveform generation using semiconductor laser for radar and microwave applications," *IEEE J. Quantum Electron.*, vol. 40, no. 6, pp. 682–689, Jun. 2004.

[9] S. Tang, R. Vicente, M. C. Chiang, C. R. Mirasso, and J. M. Liu, "Nonlinear dynamics of semiconductor lasers with mutual optoelectronic coupling," *IEEE J. Sel. Topics Quantum Electron.*, vol. 10, no. 5, pp. 936–943, Sep./Oct. 2004.

[10] S. Tang and J. M. Liu, "Chaos synchronization in semiconductor lasers with optoelectronic feedback," *IEEE J. Quantum Electron.*, vol. 39, no. 6, pp. 708–715, Jun. 2003.

[11] L. Chrostowski *et al.*, "40 GHz bandwidth and 64 GHz resonance frequency in injection-locked 1.55 μm VCSELs," *IEEE J. Sel. Topics Quantum Electron.*, vol. 13, no. 5, pp. 1200–1208, Sep./Oct. 2007.

[12] T. B. Simpson, J. M. Liu, A. Gavrielides, V. Kovanis, and P. M. Alsing, "Period-doubling route to chaos in a semiconductor laser subject to optical injection," *Appl. Phys. Lett.*, vol. 64, pp. 3539–3541, Jun. 1994.

[13] S. K. Hwang and D. H. Liang, "Effects of linewidth enhancement factor on period-one oscillations of optically injected semiconductor lasers," *Appl. Phys. Lett.*, vol. 89, pp. 061120-1–061120-3, Aug. 2006.

[14] Y. S. Juan and F. Y. Lin, "Ultra broadband microwave frequency combs generated by an optical pulse-injected semiconductor laser," *Opt. Exp.*, vol. 17, pp. 18596–18605, Sep. 2009.

[15] C. H. Cheng, Y. C. Chen, and F.-Y. Lin, "Chaos time delay signature suppression and bandwidth enhancement by electrical heterodyning," *Opt. Exp.*, vol. 23, pp. 2308–2319, Jan. 2015.

[16] L. F. Lester, N. A. Naderi, F. Grillot, R. Raghunathan, and V. Kovanis, "Strong optical injection and the differential gain in a quantum dash laser," *Opt. Exp.*, vol. 22, no. 6, pp. 7222–7228, Mar. 2014.

[17] F. Grillot, N. A. Naderi, M. Pochet, C. Y. Lin, and L. F. Lester, "Variation of the feedback sensitivity in a 1.55 μm inas/inp quantum-dash fabry–perot semiconductor laser," *Appl. Phys. Lett.*, vol. 93, no. 19, pp. 191108-1–191108-3, Nov. 2008.

[18] V. Annovazzi-Lodi, G. Aromataris, M. Benedetti, and S. Merlo, "Secure chaotic transmission on a free-space optics data link," *IEEE J. Quantum Electron.*, vol. 44, no. 11, pp. 1089–1095, Nov. 2008.

[19] V. Annovazzi-Lodi, A. Scire, M. Sorel, and S. Donati, "Dynamic behavior and locking of a semiconductor laser subjected to external injection," *IEEE J. Quantum Electron.*, vol. 34, no. 12, pp. 2350–2357, Dec. 1998.

[20] S. Donati and S. K. Hwang, "Chaos and high-level dynamics in coupled lasers and their applications," *Prog. Quantum Electron.*, vol. 36, pp. 293–341, Jul. 2012.

[21] S. Donati, "Developing self-mixing interferometry for instrumentation and measurements," *Laser Photon. Rev.*, vol. 6, pp. 393–417, Mar. 2012.

[22] V. Annovazzi-Lodi, S. Merlo, M. Norgia, and A. Scire, "Characterization of a chaotic telecommunication laser for different fiber cavity lengths," *IEEE J. Quantum Electron.*, vol. 38, no. 9, pp. 1171–1177, Sep. 2002.

[23] A. Prasad, Y. C. Lai, A. Gavrielides, and V. Kovanis, "Complicated basins in external-cavity semiconductor lasers," *Phys. Lett. A*, vol. 314, pp. 44–50, Jul. 2003.

[24] F. Y. Lin and J. M. Liu, "Chaotic lidar," *IEEE J. Sel. Topics Quantum Electron.*, vol. 10, no. 5, pp. 991–997, Sep./Oct. 2004.

[25] J. P. Zhuang and S. C. Chan, "Phase noise characteristics of microwave signals generated by semiconductor laser dynamics," *Opt. Exp.*, vol. 23, pp. 2777–2797, Jan. 2015.

[26] M. Premaratne, A. J. Lowery, Z. Ahmed, and D. Novak, "Modeling noise and modulation performance of fiber grating external cavity lasers," *IEEE J. Sel. Topics Quantum Electron.*, vol. 3, no. 2, pp. 290–303, Apr. 1997.

[27] A. P. A. Fischer, M. Yousefi, D. Lenstra, M. W. Carter, and G. Vemuri, "Experimental and theoretical study of semiconductor laser dynamics due to filtered optical feedback," *IEEE J. Sel. Topics Quantum Electron.*, vol. 10, no. 5, pp. 944–954, Sep./Oct. 2004.

[28] A. P. A. Fischer, O. K. Andersen, M. Yousefi, S. Stolte, and D. Lenstra, "Experimental and theoretical study of filtered optical feedback in a semiconductor laser," *IEEE J. Quantum Electron.*, vol. 36, no. 3, pp. 375–384, Mar. 2000.

[29] A. Naumenko, P. Besnard, N. Loiko, G. Ughetto, and J. C. Bertreux, "Characteristics of a semiconductor laser coupled with a fiber bragg grating with arbitrary amount of feedback," *IEEE J. Quantum Electron.*, vol. 39, no. 10, pp. 1216–1228, Oct. 2003.

[30] M. Yousefi and D. Lenstra, "Dynamical behavior of a semiconductor laser with filtered external optical feedback," *IEEE J. Quantum Electron.*, vol. 35, no. 6, pp. 970–976, Jun. 1999.

[31] B. Docter *et al.*, "Discretely tunable laser based on filtered feedback for telecommunication applications," *IEEE J. Sel. Topics Quantum Electron.*, vol. 16, no. 5, pp. 1405–1412, 2010.

[32] Y. Hong, P. Spencer, and K. A. Shore, "Wideband chaos with time-delay concealment in vertical-cavity surface-emitting lasers with optical feedback and injection," *IEEE J. Quantum Electron.*, vol. 50, no. 4, pp. 236–242, Apr. 2014.

[33] S. Priyadarshi, Y. Hong, I. Pierce, and K. A. Shore, "Experimental investigations of time-delay signature concealment in chaotic external cavity VCSELs subject to variable optical polarization angle of feedback," *IEEE J. Sel. Topics Quantum Electron.*, vol. 19, no. 4, p. 1700707, Jul./Aug. 2013.

[34] Y. Wu, Y. C. Wang, P. Li, A. B. Wang, and M. J. Zhang, "Can fixed time delay signature be concealed in chaotic semiconductor laser with optical feedback?" *IEEE J. Quantum Electron.*, vol. 48, no. 11, pp. 1371–1379, Nov. 2012.

[35] J. G. Wu, G. Q. Xia, and Z. M. Wu, "Suppression of time delay signatures of chaotic output in a semiconductor laser with double optical feedback," *Opt. Exp.*, vol. 17, pp. 20124–20133, Oct. 2009.

[36] F. Ruiz-Oliveras, M. C. Soriano, P. Colet, and C. R. Mirasso, "Information encoding and decoding using unidirectionally coupled chaotic semiconductor lasers subject to filtered optical feedback," *IEEE J. Quantum Electron.*, vol. 45, no. 8, pp. 972–978, Aug. 2009.

[37] N. Li *et al.*, "Statistics of the optical intensity of a chaotic external-cavity DFB laser," *Opt. Lett.*, vol. 39, pp. 5949–5952, Oct. 2014.

[38] D. Rontani, A. Locquet, M. Sciamanna, and D. S. Citrin, "Loss of time-delay signature in the chaotic output of a semiconductor laser with optical feedback," *Opt. Lett.*, vol. 32, pp. 2960–2962, Oct. 2007.

[39] D. Rontani, A. Locquet, M. Sciamanna, D. S. Citrin, and S. Ortin, "Time-delay identification in a chaotic semiconductor laser with optical feedback: a dynamical point of view," *IEEE J. Quantum Electron.*, vol. 45, no. 7, pp. 879–1891, Jul. 2009.

[40] R. Vicente, J. Dauden, P. Colet, and R. Toral, "Analysis and characterization of the hyperchaos generated by a semiconductor laser subject to a delayed feedback loop," *IEEE J. Quantum Electron.*, vol. 41, no. 4, pp. 541–548, Apr. 2005.

[41] J. Hizanidis, S. Deligiannidis, A. Bogris, and D. Syvridis, "Enhancement of chaos encryption potential by combining all-optical and electrooptical chaos generators," *IEEE J. Quantum Electron.*, vol. 46, no. 11, pp. 1642–1649, Nov. 2010.

[42] M. C. Soriano, L. Zunino, O. A. Rosso, I. Fischer, and C. R. Mirasso, "Time scales of a chaotic semiconductor laser with optical feedback under the lens of a permutation information analysis," *IEEE J. Quantum Electron.*, vol. 47, no. 2, pp. 252–261, Feb. 2011.

[43] M. J. Bunner, M. Popp, T. Meyer, A. Kittel, and J. Parisi, "Tool to recover scalar time-delay systems from experimental time series," *Phys. Rev. E*, vol. 54, pp. R3082–R3085, Oct. 1996.

[44] V. S. Udaltsov *et al.*, "Cracking chaos-based encryption systems ruled by nonlinear time delay differential equations," *Phys. Lett. A*, vol. 308, pp. 54–60, 2003.

[45] X. Porte *et al.*, "Autocorrelation properties of chaotic delay dynamical systems: A study on semiconductor lasers," *Phys. Rev. E*, vol. 90, pp. 052911-1–052911-10, Nov. 2014.

[46] R. M. Nguimdo, G. Verschaffelt, J. Danckaert, and G. Van der Sande, "Loss of time-delay signature in chaotic semiconductor ring lasers," *Opt. Lett.*, vol. 37, pp. 2541–2543, Jun. 2012.

[47] R. M. Nguimdo, M. C. Soriano, and P. Colet, "Role of the phase in the identification of delay time in semiconductor lasers with optical feedback," *Opt. Lett.*, vol. 36, pp. 4332–4334, Nov. 2011.

[48] J. G. Wu, Z. M. Wu, G. Q. Xia, and G. Y. Feng, "Evolution of time delay signature of chaos generated in a mutually delay-coupled semiconductor lasers system," *Opt. Exp.*, vol. 20, pp. 1741–1753, Jan. 2012.

[49] N. Li *et al.*, "Loss of time delay signature in broadband cascade-coupled semiconductor lasers," *IEEE Photon. Technol. Lett.*, vol. 24, no. 3, pp. 2187–2190, Dec. 2012.

[50] S. Sunada *et al.*, "Chaos laser chips with delayed optical feedback using a passive ring waveguide," *Opt. Exp.*, vol. 19, pp. 5713–5724, Mar. 2011.

[51] S. S. Li, Q. Liu, and S. C. Chan, "Distributed feedbacks for time-delay signature suppression of chaos generated from a semiconductor laser," *IEEE Photon. J.*, vol. 4, no. 5, pp. 1930–1935, Oct. 2012.

[52] A. Wang *et al.*, "Generation of wideband chaos with suppressed time-delay signature by delayed self-interference," *Opt. Exp.*, vol. 21, pp. 8701–8710, Apr. 2013.

[53] K. Hirano *et al.*, "Characteristics of fast physical random bit generation using chaotic semiconductor lasers," *IEEE J. Quantum Electron.*, vol. 45, no. 11, pp. 1367–1379, Nov. 2009.

[54] Y. Hong, "Experimental study of time-delay signature of chaos in mutually coupled vertical-cavity surface-emitting lasers subject to polarization optical injection," *Opt. Exp.*, vol. 21, pp. 17894–17903, Jul. 2013.

[55] J. G. Wu *et al.*, "Simultaneous generation of two sets of time delay signature eliminated chaotic signals by using mutually coupled semiconductor lasers," *IEEE Photon. Technol. Lett.*, vol. 23, no. 12, pp. 759–761, Jun. 2011.

[56] H. Lin, Y. Hong, and K. A. Shore, "Experimental study of time-delay signatures in vertical-cavity surface-emitting lasers subject to double-cavity polarization-rotated optical feedback," *J. Lightw. Technol.*, vol. 32, no. 9, pp. 1829–1836, May 2014.

[57] S. Y. Xiang *et al.*, "Quantifying chaotic unpredictability of vertical-cavity surface-emitting lasers with polarized optical feedback via permutation entropy," *IEEE J. Sel. Topics Quantum Electron.*, vol. 17, no. 5, pp. 1212–1219, Sep./Oct. 2011.
[58] Y. Li *et al.*, "Time-delay signature of chaos in 1550 nm VCSELs with variable-polarization FBG feedback," *Opt. Exp.*, vol. 22, pp. 19610–19620, Aug. 2014.
[59] J. Zhao *et al.*, "Stability of a monolithic integrated filtered-feedback laser," *Opt. Exp.*, vol. 20, pp. B270–B278, Jan. 2012.
[60] N. Matuschek, T. Pliska, and N. Lichtenstein, "Properties of pump-laser modules exposed to polarization-dependent and wavelength-selective feedback from fiber Bragg gratings," *IEEE J. Quantum Electron.*, vol. 44, no. 3, pp. 262–274, Mar. 2008.
[61] R. Lang and K. Kobayashi, "External optical feedback effects on semiconductor injection laser properties," *IEEE J. Quantum Electron.*, vol. 16, no. 3, pp. 347–355, Mar. 1980.
[62] S. C. Chan, S. K. Hwang, and J. M. Liu, "Period-one oscillation for photonic microwave transmission using an optically injected semiconductor laser," *Opt. Exp.*, vol. 15, pp. 14921–14935, Oct. 2007.
[63] S. K. Hwang, J. M. Liu, and J. K. White, "Characteristics of period-one oscillations in semiconductor lasers subject to optical injection," *IEEE J. Sel. Topics Quantum Electron.*, vol. 10, no. 5, pp. 974–981, Sep./Oct. 2004.
[64] S. C. Chan, "Analysis of an optically injected semiconductor laser for microwave generation," *IEEE J. Quantum Electron.*, vol. 46, no. 3, pp. 421–428, Mar. 2010.
[65] T. Erdogan, "Fiber grating spectra," *J. Lightw. Technol.*, vol. 15, no. 8, pp. 1277–1294, Aug. 1997.
[66] C. Cui and S. C. Chan, "Performance analysis on using period-one oscillation of optically injected semiconductor lasers for radio-over-fiber uplinks," *IEEE J. Quantum Electron.*, vol. 48, no. 4, pp. 490–499, Jan. 2012.
[67] F. Y. Lin and J. M. Liu, "Nonlinear dynamics of a semiconductor laser with delayed negative optoelectronic feedback," *IEEE J. Quantum Electron.*, vol. 39, no. 4, pp. 562–568, Apr. 2003.
[68] H. Erzgraber and B. Krauskopf, "Dynamics of a filtered-feedback laser: Influence of the filter width," *Opt. Lett.*, vol. 32, pp. 2441–2443, Aug. 2007.
[69] J. Ohtsubo, "Chaos synchronization and chaotic signal masking in semiconductor lasers with optical feedback," *IEEE J. Quantum Electron.*, vol. 38, no. 9, pp. 1141–1154, Sep. 2002.
[70] I. V. Ermakov, V. Z. Tronciu, P. Colet, and C. R. Mirasso, "Controlling the unstable emission of a semiconductor laser subject to conventional optical feedback with a filtered feedback branch," *Opt. Exp.*, vol. 17, pp. 8749–8755, May 2009.
[71] F. Y. Lin, Y. K. Chao, and T. C. Wu, "Effective bandwidths of broadband chaotic signals," *IEEE J. Quantum Electron.*, vol. 48, no. 8, pp. 1010–1014, May 2012.
[72] F. Grillot, B. Dagens, J. G. Provost, H. Su, and L. F. Lester, "Gain compression and above-threshold linewidth enhancement factor in 1.3-inas–gaas quantum-dot lasers," *IEEE J. Quantum Electron.*, vol. 44, no. 10, pp. 946–951, Oct. 2008.
[73] X. Z. Li and S. C. Chan, "Heterodyne random bit generation using an optically injected semiconductor laser in chaos," *IEEE J. Quantum Electron.*, vol. 49, no. 10, pp. 829–838, Oct. 2013.
[74] J. Ohtsubo, *Semiconductor Lasers: Stability, Instability and Chaos*, vol. 111, New York, NY, USA: Taylor & Francis, 2006.
[75] L. E. Larson, J. M. Liu, and L. S. Tsimring, *Digital Communications Using Chaos and Nonlinear Dynamics,* New York, NY, USA: Springer, 2006.

Song-Sui Li received the B.Eng. degree in communication engineering from the University of Electronic Science and Technology of China, Chengdu, China, in 2009. He is currently working toward the Ph.D. degree in electronic engineering with the City University of Hong Kong, Hong Kong, China. He has worked as a Radio-frequency Engineer in China Electronics Corporation during 2009–2011. His current research interests include laser nonlinear dynamics, grating-assisted optical chaos generation, and photonic microwave generation.

Sze-Chun Chan received the B.Eng. degree in electrical and electronic engineering from the University of Hong Kong, Hong Kong, China, in 2001, and the M.S. and Ph.D. degrees in electrical engineering from the University of California at Los Angeles (UCLA) in 2004 and 2007, respectively. He is currently an Associate Professor in the Department of Electronic Engineering and the State Key Laboratory of Millimeter Waves, City University of Hong Kong, Hong Kong, China. He received the Dr. Bor-Uei Chen Scholarship of the Photonics Society of Chinese-Americans in 2007. He served as one of the Guest Editors of the IEEE JOURNAL OF SELECTED TOPICS IN QUANTUM ELECTRONICS (Issue on Semiconductor Lasers 2013) and a Guest Associate Editor of the *International Journal of Bifurcation and Chaos* since 2010. His research interests include nonlinear dynamics of semiconductor lasers, optical chaos generation, radio-over-fiber, and photonic microwave generation.